

UC Santa Barbara

UC Santa Barbara Previously Published Works

Title

Evidence for competing proton-transfer and hydrogen-transfer reactions in the S1 state of indigo

Permalink

<https://escholarship.org/uc/item/5347m0vb>

Authors

Haggmark, Michael R
Gate, Gregory
Boldissar, Samuel
et al.

Publication Date

2018-11-01

DOI

10.1016/j.chemphys.2018.09.027

Peer reviewed

Evidence for competing proton-transfer and hydrogen-transfer reactions in the S₁ state of indigo

Michael R. Haggmark¹, Gregory Gate¹, Samuel Boldissar¹, Jacob Berenbeim¹, Andrzej L. Sobolewski^{2*}, and Mattanjah S. de Vries^{1*}

¹ *Department of Chemistry and Biochemistry, University of California, Santa Barbara, CA 93016-9510*

² *Institute of Physics, Polish Academy of Sciences, Al. Lotnikow 32/46, PL-02668 Warsaw, Poland*

Abstract

Indigo is a blue dye molecule that has been used since antiquity, although it is better known today for its use in blue jeans. Indigo has previously been shown to exhibit remarkable photostability due to fast excited state dynamics mediated by an excited state intramolecular proton transfer. Study of this process is complicated by the fact that the photophysics of indigo is very sensitive to the environment. In order to disentangle the intrinsic photodynamics of indigo from the effects contributed by the environment, we studied indigo in a molecular beam using resonance enhanced multiphoton ionization. We obtained excited state lifetimes of individual vibronic bands with pump-probe spectroscopy ranging from 60 ps to 24 ns. We have mapped a barrier to relaxation at about 700 cm⁻¹, beyond which fast excited state dynamics dominate. Below this barrier two decay processes compete and mode-specific relaxation occurs with certain vibronic bands near the origin relaxing faster than others, or exhibiting different partitioning between the two relaxation channels. Computational studies at the ADC(2)/MP2/cc-pVDZ level indicate that two low-barrier reaction paths exist in the S₁ state of indigo, one corresponding to proton transfer, the other to hydrogen transfer. In both cases the charge distribution changes drastically upon de-excitation. These data provide a sensitive probe of the potential energy landscape, responsible for the response to absorption of light. The results may help in understanding the photostability that preserves the blue color of indigo dyes.

1. Introduction

The blue dye, indigo, is one of the oldest, and still one of the most widely used dyes. It was used by many ancient cultures from the Egyptians, to the Romans, to the Mayans, and remarkably, artifacts from those societies still retain their blue color to this day [1, 2]. This lack of fading is due to indigo's high photostability [3].

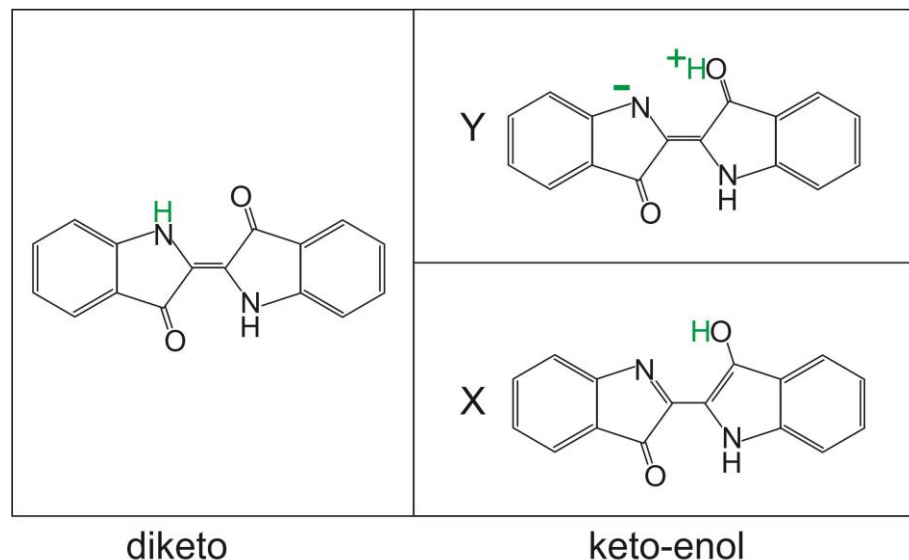
Generally speaking, photostability is granted by a process that returns a molecule to the ground state at a faster timescale than formation of reactive species [4]. For Indigo, the mechanism providing fast return to the ground state is thought to be due to an excited-stated intramolecular

proton transfer (ESIPT), first studied computationally in-depth by Yamakazi et. al, [5] who found a very short excited state lifetime due to ESIPT from a diketo to a keto-enol tautomer. Moreno et. al further examined the relaxation pathway through conical intersections (CI) [6], finding agreement with experimental work. Another possible relaxation process is photoisomerization, which has been shown to only occur when the proton transfer coordinate is blocked [7-9]. A number of studies have attempted to unambiguously observe proton transfer for indigo. Photoelectron spectroscopy of an indigo derivative, indigo carmine, found that the excited-state lifetime in the gas-phase was around 1 ps [10]. Time resolved spectroscopy of an indigo analogue that only allowed a single proton transfer revealed a fluorescence spectrum with a biexponential decay, hinting at fluorescence from two different states, possibly the diketo (KK) and keto-enol (KE) states [11]. Transient absorption spectroscopy of indigo in DMSO revealed a lifetime on the order of 120 ps, but showed no evidence of proton transfer (PT) [12]. Iwakura et. al used sub-5 fs resolution coherence experiments to directly observe the new vibrational modes that arise from PT in indigo-carmine [13, 14]. Seixas et al. reported a significant blue-shift in the absorption spectrum and an increase in fluorescence quantum yield was seen between indigo and its leuco (reduced) form, due to a slowing down of the relaxation process and increasing competitiveness of the radiative pathway [15]. The fluorescence spectrum of leuco indigo increased and slightly shifted with prolonged light exposure, thought to be due to photoisomerization [16]. Studies with deuterated indigo and analogues to observe and measure the tunneling mechanism in PT showed an increase in the lifetime with deuteration, consistent with a tunneling assisted proton transfer mechanism [10, 14].

PT is the process of transferring a proton from one molecular moiety to another along an intramolecular hydrogen bridge. A commonly accepted paradigm presumes this situation pertains to the process that occurs in the ground state of a molecular system and often the acronym GSIPT (ground-state intramolecular PT) is assigned to this phenomenon. On the other hand, in the excited electronic state transfer of a proton between molecular moieties is accompanied by transfer of an electron, and often this phenomenon is called ESIHT (excited-state intramolecular hydrogen transfer). The tautomers generated by these processes are illustrated in Scheme 1.

Yamazaki et al. and Moreno et al. proposed that the single proton transfer from the diketo to the mono-enol tautomer affects the potential energy surfaces (PES), allowing the excited state and ground state energies to intersect and form a CI [5, 6]. After ultrafast internal conversion through the CI, the ground state keto-enol will transfer the proton back, reforming the diketo tautomer and ground state equilibrium geometry. If there is a barrier in the excited state, the proton will have to tunnel through to successfully transfer. The occurrence of a barrier and tunneling implies that the PES has a double-well potential. Tunneling describes the behavior of the proton quantum mechanically, while classically, the proton has to go over the barrier. Therefore, the probability of proton transfer is dependent on the barrier height and width. The barrier height and width are dependent on the distance between the proton donor N and the acceptor O atoms [17]. This is one of the most relevant reaction coordinates [18]. The other significant reaction coordinate is the N-H distance. Dynamical effects, such as vibrational motions, can modulate barrier width and height and significantly affect tunneling probability. Therefore, the tunneling rate is dependent on three factors: (1) total amount of excess energy imparted, (2) specific mode excitation, and (3) internal vibrational redistribution (IVR) of energy to occupy relevant modes [18].

In this study, we confirm the presence of the diketo tautomer of indigo in the gas phase and measure the lifetime of the excited state at various excess energies to generate a picture of the height of the barrier. This work aims to further explore the photostability of indigo and elucidate the main relaxation pathways in the gas phase.



Scheme 1. Tautomeric structures of indigo pertaining to this work.

2. Methods

Experimental

The experimental setup has been described in detail elsewhere [19], and only a short description follows. Indigo (Sigma, 95%) is placed on a translating graphite bar and desorbed via a focused Nd:YAG pulse (1064 nm, ~1 mJ/pulse) operating at 10 Hz. Supersonic jet cooling from an argon molecular beam (8 atm backing pressure, 30 μ s pulse width) entrains the gaseous molecules, quickly cooling them. These cold, gaseous molecules are then ionized using resonant two photon ionization (R2PI) and directed into a reflectron time-of-flight mass spectrometer.

Two-color resonant two-photon ionization (2C-R2PI) is performed using an EKSPLA PL2251 Nd:YAG laser system producing ~30 ps pulses. The 355 nm output pumps the EKSPLA PG-401 tunable optical parametric generator (OPG) (visible output of ~.5mJ). Residual 1064 nm and 532 nm light from the pump are mixed to harmonically generate 213 nm (0.3mJ), which is used as the ionization pulse.

IR light is generated using a Laser Vision tunable optical parametric oscillator/optical parametric amplifier (OPO/OPA) (mid-IR output over the range 3000-3800 cm^{-1} of ~1-2 mJ/pulse, 3 cm^{-1} spectral line width). IR light precedes the excitation/ionization pulses by ~200 ns. Two variations of IR double resonant spectroscopy are used. In mode I, the IR laser scans across IR wavelengths, while the ionization pulse is held constant at a resonant R2PI transition for a given

tautomer. The IR pulse burns out the cold, ground state molecules whenever it hits a vibrational resonance, taking the excitation pulse out of resonance and causing a decrease in signal. This will produce the IR spectrum for the specific tautomer that is being ionized. In mode II, the IR pulse is held constant at a resonant vibrational transition, while the ionization pulse scans the R2PI spectrum. In this way, a tautomer is labeled by a vibrational stretch and signal decreases whenever the transition is shared. All double resonance spectroscopic experiments are chopped to compare the experimental “burn” signal to control signal *in situ*, with alternating shots collecting burn and control signals.

Pump-probe experiments are performed in both the picosecond and nanosecond regimes. In the picosecond regime, the 30 ps pump pulse from the OPG laser system is tuned to a resonant transition, while the probe is the 5th harmonic (213 nm) from the pump laser for the OPG. The 5th harmonic can be mechanically delayed up to ~1.5 ns in time, relative to the OPG pulse, for picosecond pump-probe measurements. In the nanosecond regime, pump pulse is again from the OPG and tuned to a resonant transition, but the probe pulse is from an excimer laser (193 nm, 1.5-2 mJ/pulse, 6ns pulsewidth). To account for ionization laser difference, several nanosecond pump probes were also measured by tuning a dye laser (Lumonics HD300 ~.5mJ) to a resonant transition and probing with the 213 nm light from the ps pump laser. No difference was observed in the ns pump-probe results between 213 nm and 193 nm probe laser wavelengths. Visible-visible hole burning was also performed in an analogous manner to mode II IR by tuning the dye laser to the origin transition ~200 ns prior in time and scanning the OPG across the region of interest to verify only a single tautomer was present.

Pump-probe measurements are taken in two time regimes to help determine what processes are occurring in the excited state. By combining information from both time regimes and observing the changes in lifetime with varying excess energy, conclusions can be drawn about the excited state dynamics. The method for deriving lifetimes is based on previous work, and explained in more detail there.[20] Briefly, lifetimes are derived from kinetic equations and solving the system of ordinary differential equations. This procedure involves convolving the instrument response function (IRF) with a mono- or bi-exponential decay function. The IRF is represented by a Gaussian function centered around t_0 .

Computational

The ground-state tautomers of indigo were optimized and harmonic frequencies calculated using second order Moller-Plesset perturbation theory (MP2) with the cc-pVDZ basis set in Gaussian 09 [21]. A scaling factor of 0.95 and a 2cm^{-1} Lorentzian width were applied for the simulated IR spectra. Ground state energies of isomers/tautomers have been zero-point energy (ZPE) corrected.

Excitation energies, excited-state reaction paths and energy profiles were calculated with the second-order algebraic-diagrammatic-construction (ADC(2)) method [22, 23]. The reaction path for the ES IPT reaction was constructed as a so-called relaxed scan, that is, for a fixed value of the driving coordinate (the NH distance for PT reaction and CCCC dihedral angle for inter-ring twist) all other internal coordinates of the molecule were relaxed in the S_1 state. The approximate reaction path between the two (X and Y) excited-state conformers of the mono-enol form of

indigo was constructed as a linear interpolation in internal nuclear coordinates between equilibrium geometries of both structures. The energy profiles of this reaction path were obtained as single-point energy calculations along the interpolated path.

The MP2 and ADC(2) calculations were carried out with the TURBOMOLE program package, [24] making use of the resolution-of-the-identity (RI) approximation [25] for the evaluation of the electron-repulsion integrals. The cc-pVDZ basis set was used for all calculations.

3. Results

Experimental

Figure 1 shows the 2C-R2PI spectrum of indigo (black trace). The excitation laser is the same in both panels but the ionization laser is 193 nm/6 ns in the top panel and 213 nm/30 ps in the bottom panel. R2PI was collected with different pulse widths to show the probing ability of the laser systems in different time domains. The top trace truncates at 700 cm^{-1} to a lack of signal beyond that point while peaks continue to appear toward the blue in the bottom trace. The origin transition appears at 18129 cm^{-1} (551.6 nm), and all excitation spectra are presented relative to it. Squares denote lifetimes obtained by pump probe spectroscopy for both the ns (green) and ps (blue) time domains. Figure 2 shows individual pump probe transients of the first two peaks. Figures S1-4 show additional transients.

Figure 3 shows the IR spectrum obtained by IR-Vis double resonance spectroscopy mode I. Peaks at 3084 and 3444 cm^{-1} , correspond to overlapping C-H modes and the N-H stretch, respectively. We did not observe any additional peaks further to the blue, up to 3800 cm^{-1} . These results agree with the computations, matching the calculated trans-diketo tautomer. To confirm that only the trans-diketo was present in the beam, we carried out visible-visible double resonance spectroscopy (Fig. 4) and mode II IR hole-burning (Fig. S5). From these data, we can confidently conclude that we observe only the trans-diketo tautomer in our beam.

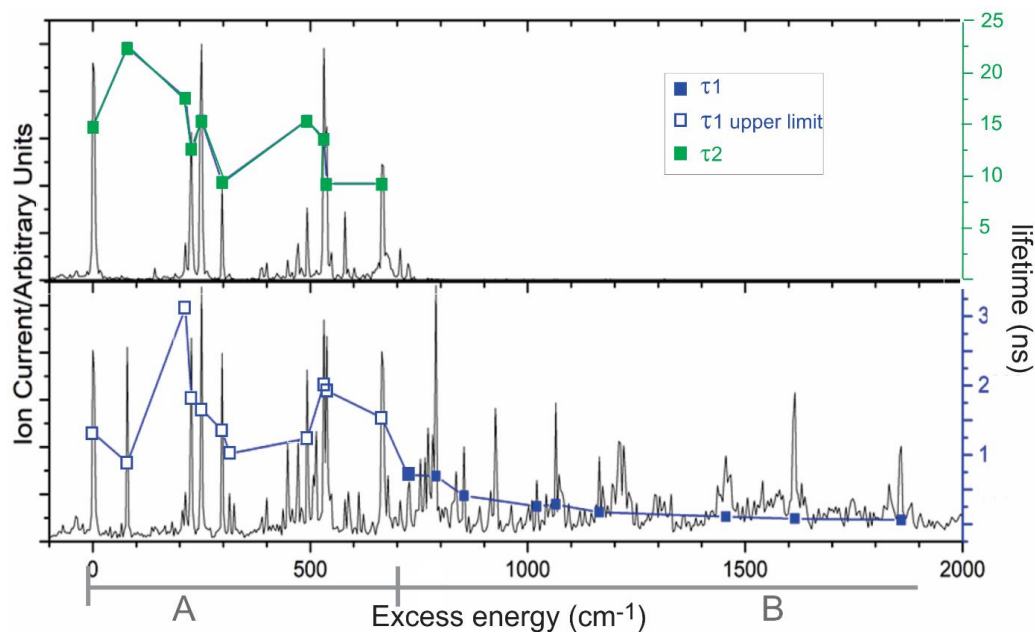


Figure 1. 2C-R2PI spectra (black) collected using ps excitation followed by ionization with 193 nm ns pulses (top panel) and 213 nm ps pulses (bottom panel). Squares denote the lifetimes as recorded from pump-probe measurements in the ns range (green) and ps range (blue). Below 700 cm^{-1} (spectral range A), the lifetimes show the presence of multiple components and only upper limits are reported for the ps pump probe experiments (see discussion). Above 700 cm^{-1} (spectral range B) we observed a single timescale component. For the ns spectra, the lasers are separated in time by a few ns.

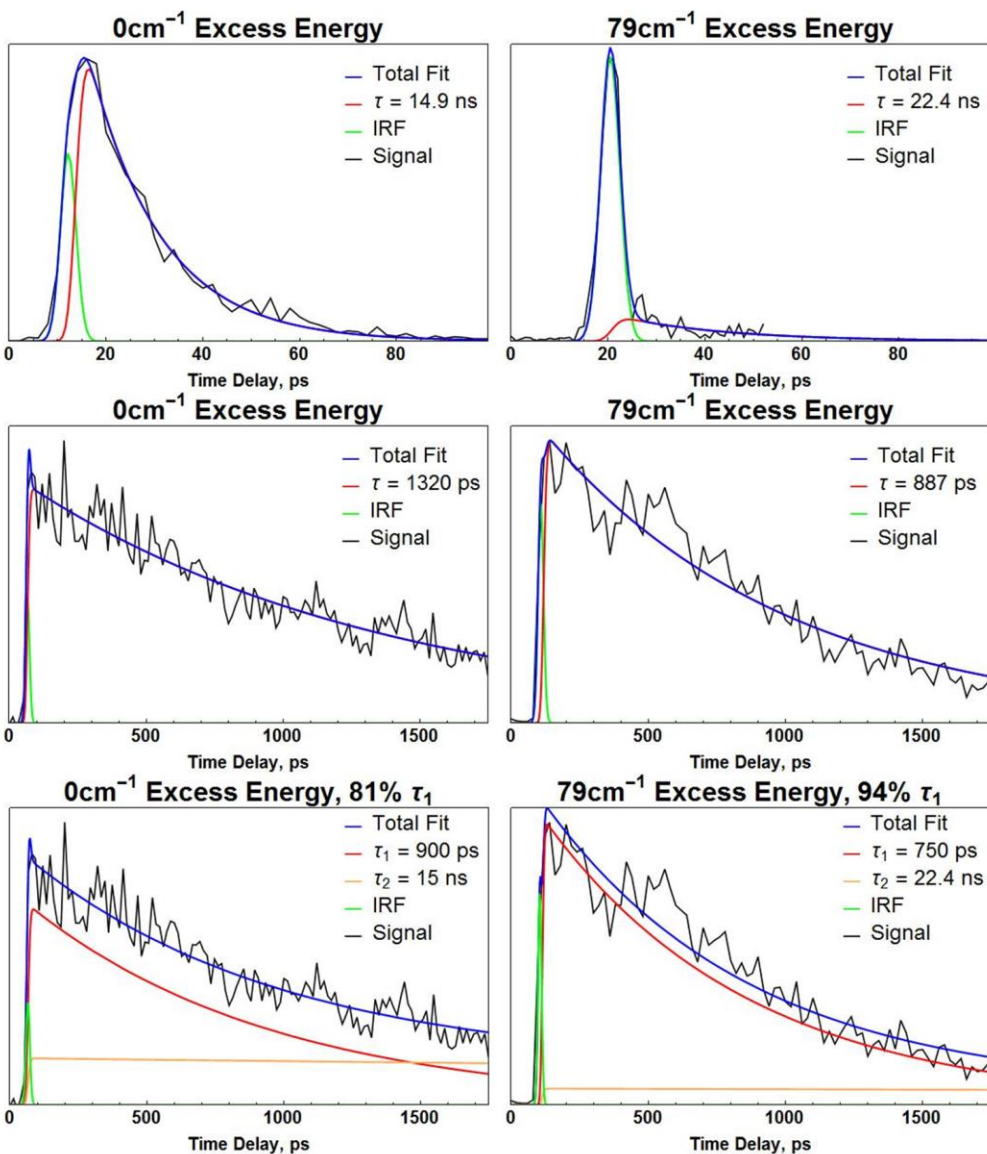


Figure 2. Pump-probe performed in the ns (top two traces) and ps (middle two traces) time domains for the origin transition and the $+79\text{cm}^{-1}$ peak. The bottom two traces show the biexponential fitting method used as an estimate for the relative quantum yields (see text). The dominant IRF feature seen in the 79 cm^{-1} ns pump probe spectrum is indicative that a faster process is the major contributor to the signal. The lack of this behavior in other peaks supports the idea of mode specific relaxation (see discussion).

Table 1 lists the lifetime values derived by fitting the results of pump probe spectroscopy. For the ns pump probe results, we fit a mono-exponential decay function to the trace. For the ps measurements we can fit with a mono-exponential function and the results appear in Table 1. However, this approach provides an upper limit for the lifetime only. The reason is that we know

from the ns measurements that there is also a slower component to the decay so at least one additional exponential needs to be included and the total decay is of the form:

$$I(t) = a_1 e^{-t/\tau_1} + a_2 e^{-t/\tau_2}$$

Here the coefficients a_1 and a_2 are the relative intensities for each of the two processes and τ_1 and τ_2 are the corresponding lifetimes. Including the second term leads to fits with smaller values of τ_1 . Assuming only two processes occur, the quantum yield for process 1 is $QY = a_1/(a_1+a_2)$. In this analysis we assume that the ionization efficiency for the two processes is the same. If that is not the case the values of a_1 and a_2 will differ.

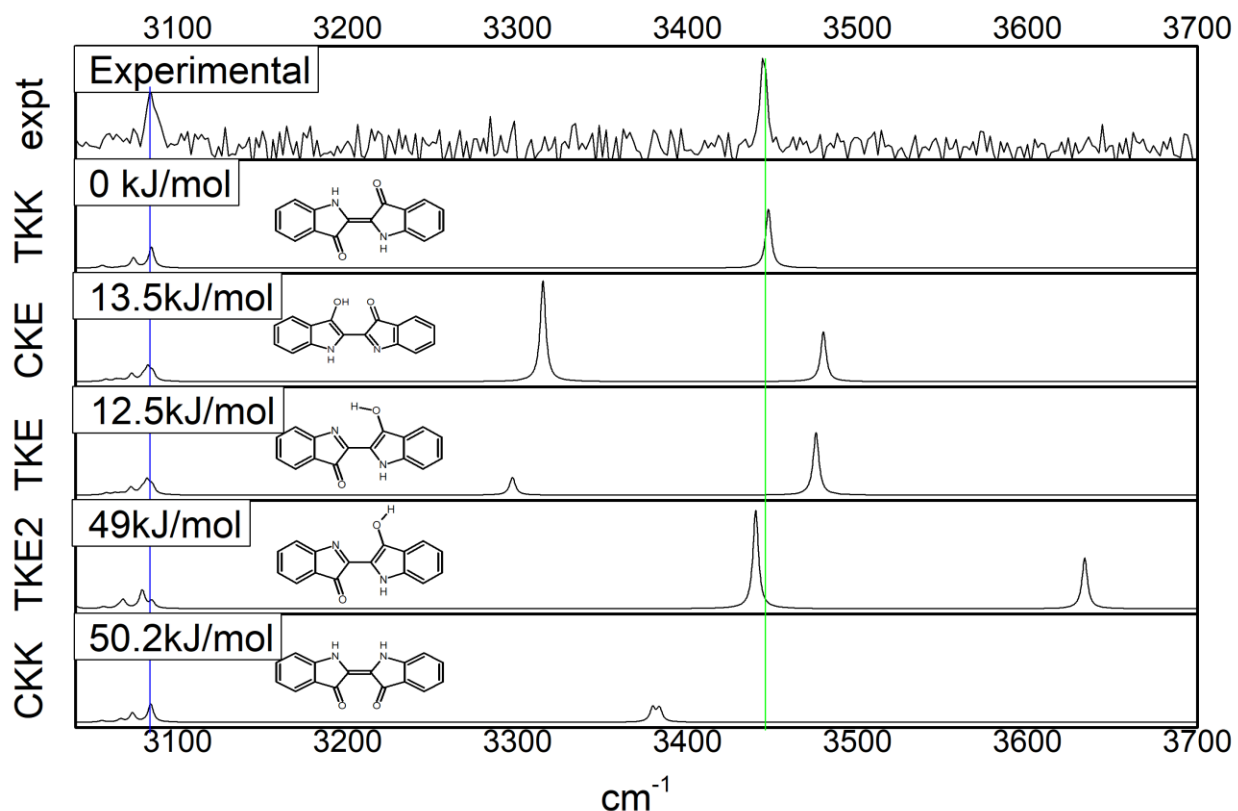


Figure 3. IR-Vis double resonance spectroscopy mode I experimental data (top panel) of indigo from 3040 – 3700 cm^{-1} . Probe was taken at the origin, 18129cm^{-1} . For comparison, the vibrational frequencies of the lowest energy tautomers are plotted with a 0.95 scaling factor applied. The abbreviations on the axes correspond to (from top to bottom) the trans diketo, cis keto-enol, trans keto-enol, trans keto-enol 2, and cis diketo tautomers.

Figure 1 and Table 1 show the mono-exponential fits for τ_1 , corresponding to $a_2 = 0$ and thus representing an upper limit of τ_1 for spectral range A. τ_1 are the lifetimes derived from the ps pump probes and τ_2 are the lifetimes derived from the ns pump probes. We know, in fact, based on the ns pump-probe results, that $a_2 > 0$ in spectral range A, with particular notice of the 79 cm^{-1} excess energy peak having a_2 very close to zero. We can fit the ps pump-probe data satisfactorily with a range of combinations of τ_1 and τ_2 to give different values of QY for process

1 (the faster decay). Table 1 lists a number of these combinations and Figure 6 gives a graphic representation of these data. We will discuss the implications of this analysis in the next section. The values of τ_2 as obtained with the 193 nm/ns ionization and 213 nm/ps ionization are identical within 0.3 ns or better, as listed in table 1, suggesting that both wavelengths probe the same excited state populations.

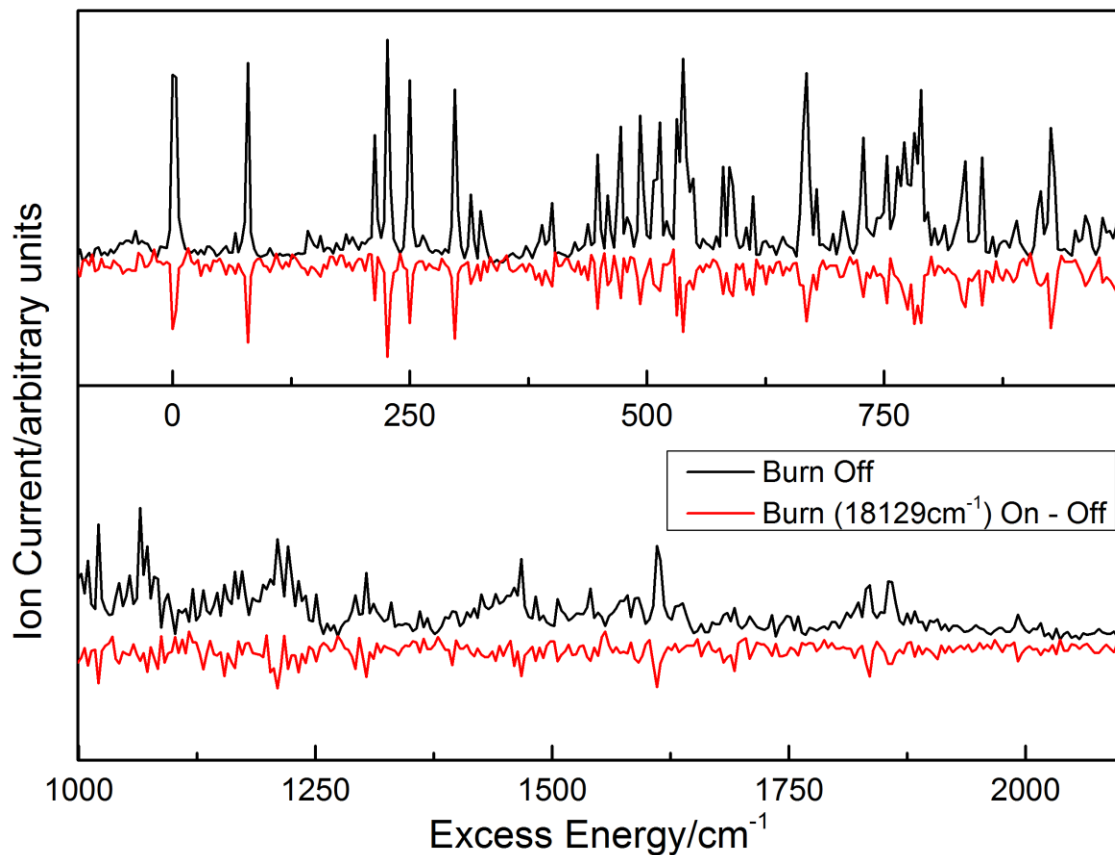


Figure 4. Visible-visible double resonance spectroscopy of indigo. The burn laser was set on the origin while the probe laser (ps OPG+213nm) was scanned and fired 200 ns later. Excited molecules were ionized with 213 nm.

peak	Peak (nm)	excess energy (cm ⁻¹)	Lifetimes (ns)			a ₁ /(a ₁ +a ₂) = QY1 in % for given values of τ ₁ in ps				
			τ ₁	τ ₂ 193 nm	τ ₂ 213 nm	750	900	1050	1200	1500
1	551.6	0	1.320	14.9	15.0	75	81	88	94	
2	549.2	79	0.887	22.4		94	100			
3	545.2	213	3.127	17.0	18.2	39	42	45	48	55
4	544.8	226	1.822	13.9	14.2	60	65	70	76	88
5	544.1	250	1.660		16.1	65	70	76	82	94
6	542.7	297	1.353	9.2	9.1	73	79	85	93	
7	542.2	314	1.019			86	93	100		
8	537	493	1.238	14.8		78	84	91	98	
9	535.9	531	2.017	13.3		57	60	64	70	
10	535.7	538	1.924	9.4		54	59	65	70	83
11	532.1	664	1.540	8.6		70	76	82	90	

Table 1: Observed ps and ns lifetimes fit with mono-exponential functions for both processes in spectral range A. 542.2 nm is a small peak in both ps and ns and we were unable to record a pump probe trace with sufficient signal to noise with the ns system. The QYs for process 1 are shown, calculated for different values of τ₁, as formulated in the text. The highlighted column is discussed in the text.

nm	excess energy/cm ⁻¹	ps lifetime monoexponential fit
530.4	725	710
528.6	789	736
526.8	853	410
522.2	1021	257
521	1065	286
518.3	1165	168
510.6	1456	105
506.5	1614	79
500.3	1859	60

Table 2: Observed lifetimes fit with mono-exponential functions in spectral range B.

Computational

We optimized two stable structures of indigo on the ground-state potential-energy (PE) surface: a diketo and a keto-enol tautomeric form. The latter, identified below as the X form, is 0.13 eV higher in energy than the former at this (MP2/cc-pVDZ) theoretical level. The diketo form is

non-polar by symmetry with a central CC bondlength of 1.378 Å (Table S1a) which is typical for a double bond in an aromatic system. The keto-enol tautomer has a dipole moment, μ_0 , of 1.40 Debye and a central CC bondlength of 1.421 Å (Table S2a). Such a relatively small change of polarity and the reversion of the single/double bond pattern suggests that the transfer of the proton is accompanied by an electron transfer leading in effect to GSIHT as discussed hereafter.

The calculated electronic absorption spectra of both tautomeric forms (see Tables S1a and S2a of the ESI) are dominated by the transition to the lowest singlet state (S_1) of the $\pi\pi^*$ orbital nature. The adiabatic energy of the S_1 state of the diketo tautomer is estimated as 2.09 eV at this theoretical level and the energy of fluorescence is estimated as 1.98 eV (Table S3a). Notably, electronic excitation of the keto-enol tautomeric form shifts electron density from the proton accepting molecular moiety back to the proton donating moiety resulting in a highly polar species ($\mu_1=6.45$ Debye, Tables S2a and S2b) which can now be classified as a proton transfer (PT) species. This observation implies that this keto-enol form has HT character in the S_0 ground state and PT character in the S_1 excited state. We are not aware of such a phenomenon having been described before in the existing very rich ESIPT related literature.

To our surprise, we found two almost isoenergetic stable forms of the keto-enol tautomer in the S_1 state by excited-state geometry optimization. These forms (denoted as X and Y) are illustrated in Scheme 1, with additional details provided in Tables S4 and S5. Both keto-enol forms exhibit well defined minima on the S_1 PE surface and are more stable than the diketo form by about 0.09 eV. The vertical energy of the ground state computed at these geometries are very different (0.436 eV for X and 1.035 eV for Y, respectively). This suggests a large difference between their equilibrium geometries.

Inspection of the most crucial geometrical parameters (bond lengths and dipole moments) shows that the X form corresponds to the keto-enol form optimized in the ground state with a similar single/double bond pattern within the central molecular unit. The X form has a central bond length of 1.454 Å compared to 1.383 Å of the Y form, or 1.397 Å of the diketo. At its S_1 -optimized equilibrium geometry (Table S4) the X form is highly polar ($\mu_1=6.77$ Debye) and its de-excitation to the ground state reduces the dipole moment to $\mu_0=1.27$ Debye. As discussed above, this behavior strongly suggests an HT type process in the S_0 state and PT type process in the S_1 state. By contrast, the electronic structure of the Y form is practically the opposite. For the Y form the ground state is more polar ($\mu_0=4.14$ Debye) than the S_1 state ($\mu_1=3.39$ Debye), cf. Table S5a. The angle between dipole moments in the S_1 state of both forms is about 125 degrees, indicating that they are polarized in different directions. These differences in the electronic structures of the X and Y forms are accompanied by differences in the nuclear geometry. In particular, the forms show different single/double bond-length patterns of the central molecular moiety, with the X form resembling the ground state keto-enol and the Y form resembling the diketo (Scheme 1 and Tables S4a and S5a). The electronic excitation of the X and Y forms only partially shifts the charge from one molecular unit to the other, as can be seen from inspection of the relevant MOs in Tables S4b and S5b, respectively, and this has almost no impact on nuclear geometry.

To estimate the barrier that separates the X and Y forms of the keto-enol tautomer in the S_1 state, we computed the PE profile along the linearly interpolated reaction path that connects their

equilibrium geometries, optimized in the S_1 state. The inset of Figure 5 shows the resulting PE profile and one can notice that estimated barrier separating the X form from the Y form on the S_1 PE surface is rather small (about 0.013eV). This indicates that in the excited state the two forms of the keto-enol tautomer represent rather two minima of a double-well potential than two separate chemical species. The Y form is unstable in the ground state and converges to the X form upon geometry optimization.

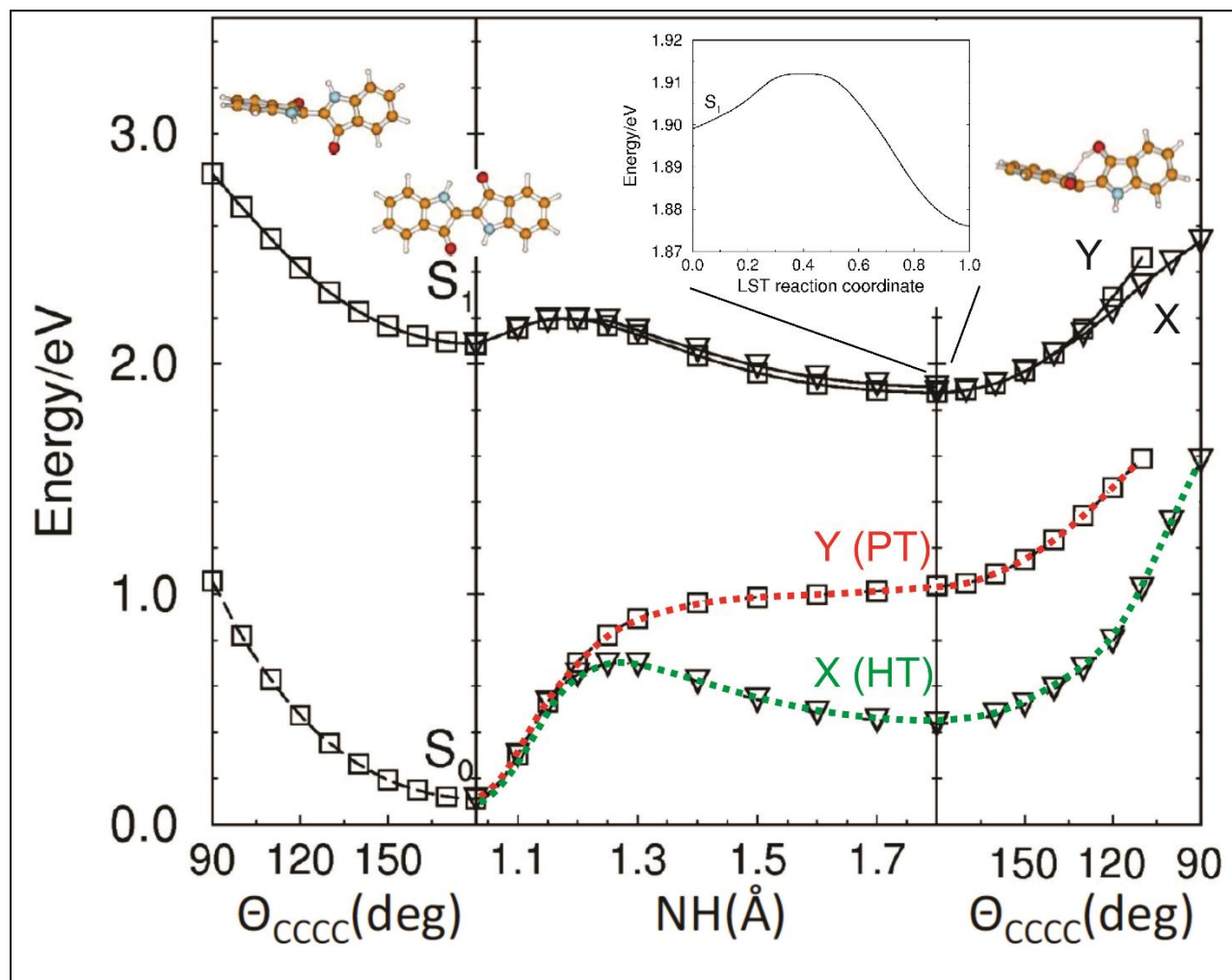


Figure 5. Potential-energy (PE) profiles of the S_0 and S_1 states of indigo computed at the ADC(2)/cc-pVDZ level of theory along the minimum-energy paths optimized in the S_1 state for the PT coordinate (NH distance)-central panel, and the inter-ring twist coordinate (CCCC dihedral angle) of the di-keto (left panel) and the keto-enol (right panel) tautomers. Solid lines denote minimum-energy profiles of the S_1 state. Dashed lines denote vertical-energy profiles of the ground state computed at the geometry of the S_1 state. PE profiles of the X and Y forms are represented by squares and triangles, respectively. The red color indicates proton transfer and the green color indicates H-atom transfer. **Inset illustrates the barrier which separates the two tautomeric forms computed along the Linear Synchronous Transit (LST) reaction path connecting the S_1 -state optimized geometries of the X (left) and Y (right) conformers.**

Figure 5 shows potential energy (PE) profiles optimized in the S_1 state along the PT coordinate (NH bond-length) and along the inter-ring twist coordinate (CCCC dihedral angle) together with PE profiles of the ground state computed along these coordinates.

Inspection of the results that are summarized in Figure 5 leads to the following conclusions:

(i) The PE profile for proton transfer in the S_1 state shows a barrier of the order of 0.11eV and the reaction is exothermic by about 0.21eV. (ii) There are two minimum-energy PE valleys that connect the diketo tautomer with the two forms of the keto-enol tautomer on the PE surface of the S_1 state. (iii) The reaction paths associated with these profiles are different as they result in different ‘vertical’ PE profiles of the ground state computed along these paths. (iv) A significant reduction of the S_1 - S_0 vertical energy gap for the Y form of the keto-enol tautomer (0.84 eV) as compared to the X form (1.47 eV) provides the source of more efficient radiationless decay of electronic excitation of the former. The process may involve tunneling through the barrier, which is apparently smaller or thinner for the Y form. Work by Yamazaki et al. [5] points to a possible CI with the ground state but the observed decays on the ps-ns timescale suggest tunneling as the more likely pathway. This conclusion is consistent with the CI at energies higher than the stable equilibria determined at the S_1 PE surface [5,6]. (v) The inter-ring twist of the diketo as well as keto-enol tautomeric forms does not lead to the intersection with the ground state as it is usually found for typical ESIPT systems (cf. [26] for instance).

4. Discussion

The visible-visible double resonance spectrum (Figure 4) and mode II IR-vis spectrum (Figure S5), confirm that all peaks observed belong to a single tautomer. Based on the mode I spectrum (Figure 3), coupled with calculations, we can assign the single tautomer observed in our beam as the trans-diketo.

To describe the excited state dynamics we distinguish two ranges of the R2PI spectrum: spectral range A below 700 cm^{-1} excess energy and spectral range B with more than 700 cm^{-1} excess energy. The pump-probe data in range A are characterized by two excited state lifetimes that strongly depend on the vibrational mode of excitation and that differ by an order of magnitude. The shorter lifetime, τ_1 , is of the order of 1 ns while the longer lifetime, τ_2 , is of the order of 10 ns. For range B we find a single lifetime of less than one ns which gradually decreases with increasing energy. We note that proton transfer is one of the fastest reactions possible. It has been found to occur in less than 1 ps [13, 14, 18]. Therefore, if proton or hydrogen transfer is involved, these lifetimes likely describe the dynamics of the keto-enol excited state or states once they are formed, rather than the dynamics of the initially excited diketo state.

The two lifetimes in range A likely correspond to two deactivation processes from two different excited states. If both channels originated from a single excited state, the slower decay would correspond to a lower rate and would probably be hard to observe in our experiment. According to the calculations as depicted in Figure 5, there are two reaction pathways leading from the diketo tautomer to the keto-enol ones on the PE surface of the S_1 state. They differ in the amount of electric charge that accompanies the proton transfer reaction. Since the S_1 PE profiles of both forms behave in a similar fashion with respect to the inter-ring torsion that does not modulate

significantly the S_1 - S_0 energy gap, we can postulate that according to the energy-gap law [27, 28] the Y form will undergo a faster decay to the ground state, but we do not have further hard evidence to confidently correlate the faster and slower process with the Y and X form, respectively. Geometrical rigidity of the indole moiety results in a relatively low density of vibrational states at low excess energy above the electronic origin of the S_1 state. Thus the low vibrational levels of indole conserve their quantum identity to a large extent and this makes their coupling to the particular channels along the PT reaction path mode sensitive.

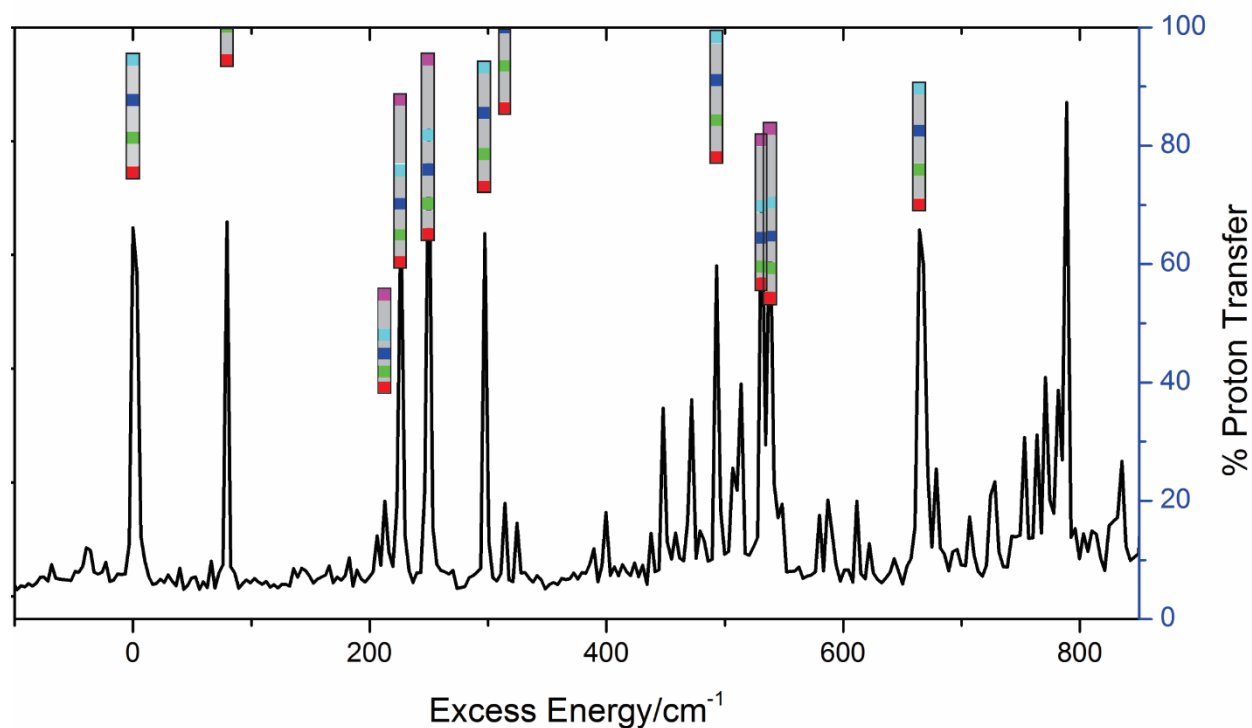


Figure 6: Graphic representation of the data in Table 1, showing QY (percent proton transfer) for specific vibronic peaks and for different values of τ_1 : red-750 ps, green-900 ps, blue-1050 ps, light blue- 1200 ps, purple-1500 ps.

The absence of the slow process beyond 700 cm^{-1} indicates that these excess energies are higher than the relevant barrier separating the Franck-Condon region from a keto-enol minimum. Below that energy, in range A, we observe two processes and beyond that energy, in range B, just one. There could be several causes for the absence of the slow process at higher excitation energies. It is possible that the slow process becomes fast or that beyond 700 cm^{-1} only the form responsible for the fast process is populated. Perhaps more likely is that the X and Y forms are able to interconvert, as IVR provides the energy to overcome the small barrier ($\sim 100\text{ cm}^{-1}$) between the two geometries. The decrease of lifetime with increasing energy in range B could be due to increasing deactivation rates, for example because of increasing internal conversion probability at higher excess energy [28].

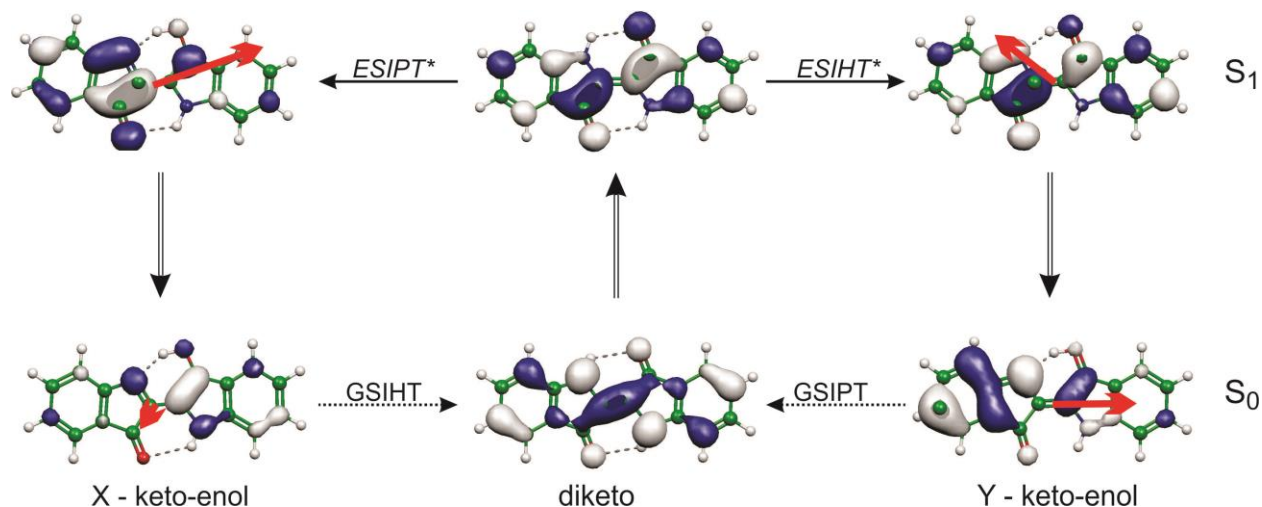


Figure 7: Diagram depicting transitions between the relevant tautomeric forms in ground state and excited state with electron orbitals involved in transitions and dipole moments (red arrows). Double arrows for electronic transitions, dotted arrows for ground state transitions, and solid arrows for transitions between forms in the excited state.

In range A we notice mode specificity evidenced by different lifetimes for different vibronic transitions. Figure 6 shows a graphic representation of the calculated QY data for the faster process from Table 1. If we assume that the fast process is the same for all modes, then a good estimate would be for it to be around 900 ps, as is the case for the $+79\text{ cm}^{-1}$ peak for which there is only a fast component. The values based on these assumptions are listed in the highlighted column of Table 1. The QY for the faster process is between 40% and 100% under all explored parameter values. Even though this is a wide range, there is no single combination of lifetime and QY that fits the data for all modes. Either the initial partitioning amongst X and Y depends strongly on the vibronic mode or so do the lifetimes of the X and Y states once they are formed. The latter would imply that the molecule in the X or Y states remember the original vibrational mode in the diketo state which would suggest slow or inefficient IVR [29, 30]. Such slow IVR would also be consistent with limited intermixing between the X and Y forms below 700 cm^{-1} , thus maintaining separate lifetimes.

Our results lead to the conclusion that indigo represents an exception among molecular systems subject to the ESIPT phenomenon, which generally is accompanied by GSIPT. In the case of indigo GSIPT leads to a structure (Y) which is unstable in S_0 while GSIHT leads to a form (X) that is stable in S_0 . In the S_1 state these processes are accompanied by a shift of electron density (rather than charge transfer) which goes in an opposite direction along the two reaction paths. As illustrated in Figure 7, optical excitation of the X keto-enol form S_0 to the S_1 state results in a partial back charge transfer from the proton-accepting to the proton-donating moiety and this both raises the dipole moment of the state and changes its direction. A reverse situation occurs for the Y form. The significant polarity of the ground state at its S_1 equilibrium geometry indicates a 'standard' proton transfer process in this state and electronic excitation partially

neutralizes the polarity of the system. Electronic excitation qualitatively reverses the dipole moment of a given conformer and the dipole moments in the S_1 state are polarized approximately in the opposite directions to those of the ground states. The estimated angle between dipole moments of the X and Y forms in the S_1 state is about 125 degrees. This observation may have consequences regarding stabilization of these forms by different polar solvents or by specific chemical modifications of the indigo core.

Summarizing, we make the following observations. Unlike in common ESIPT systems, indigo also exhibits hydrogen transfer as part of its photochemistry. Experimentally we observe two deactivation processes. Our calculations predict two pathways as well, involving PT and HT, respectively, in the excited state and the opposite character (HT and PT) in the ground state trajectories. There is a narrow spectral range (up to 700 cm^{-1} above the origin) in which the partitioning among the two pathways depends strongly on vibrational modes. Above 700 cm^{-1} the excited state lifetime shortens considerably, providing a mechanism for indigo's stability against radiative damage. We are undertaking follow-up studies with deuterated indigo to further elucidate the excited state dynamics

Acknowledgments

This work was supported by the National Science Foundation under CHE-1301305. We acknowledge support from the Center for Scientific Computing from the CNSI, MRL: an NSF MRSEC (DMR-1121053) and NSF CNS-0960316. A. L. S. acknowledges support by the Alexander von Humboldt Research Award.

References

- [1] R.J.H. Clark, C.J. Cooksey, M.A.M. Daniels, R. Withnall, Indigo, Woad, and Tyrian Purple - Important Vat Dyes from Antiquity to the Present, *Endeavour* 17 (1993) 191-199.
- [2] J.C. Splitstoser, T.D. Dillehay, J. Wouters, A. Claro, Early pre-Hispanic use of indigo blue in Peru, *Science advances* 2 (2016) e1501623.
- [3] R.M. Christie, Why is indigo blue?, *Biotech Histochem* 82 (2007) 51-56.
- [4] J.E.A. Otterstedt, Photostability and molecular structure, *The Journal of Chemical Physics* 58 (1973) 5716-5725.
- [5] S. Yamazaki, A.L. Sobolewski, W. Domcke, Molecular mechanisms of the photostability of indigo, *Phys Chem Chem Phys* 13 (2011) 1618-1628.
- [6] M. Moreno, J.M. Ortiz-Sanchez, R. Gelabert, J.M. Lluch, A theoretical study of the photochemistry of indigo in its neutral and dianionic (leucoindigo) forms, *Phys Chem Chem Phys* 15 (2013) 20236-20246.
- [7] G.M. Wyman, B.M. Zarnegar, Excited State Chemistry of Indigoid Dyes. 11. The Interaction of Thio- and Selenoindigo Dyes with Hydroxylic Compounds and Its Implications on the Photostability of Indigo, *The Journal of Physical Chemistry* 77 (1973) 1204-1207.
- [8] A.D. Kirsch, G.M. Wyman, Excited state chemistry of indigoid dyes. 5. The intermediacy of the triplet state in the direct photoisomerization and the effect of substituents, *The Journal of Physical Chemistry* 81 (1977) 413-420.
- [9] G. Miehe, P. Süsse, V. Kupcik, E. Egert, M. Nieger, G. Kunz, R. Gerke, B. Knieriem, M. Niemeyer, W. Lüttke, Light Absorption as well as Crystal and Molecular Structure of N, N'-Dimethylindigo: An Example of the Use of Synchrotron Radiation, *Angewandte Chemie International Edition in English* 30 (1991) 964-967.
- [10] A.S. Chatterley, D.A. Horke, J.R. Verlet, On the intrinsic photophysics of indigo: a time-resolved photoelectron spectroscopy study of the indigo carmine dianion, *Phys Chem Chem Phys* 14 (2012) 16155-16161.
- [11] J. Pina, D. Sarmiento, M. Accoto, P.L. Gentili, L. Vaccaro, A. Galvao, J.S. Seixas de Melo, Excited-State Proton Transfer in Indigo, *J Phys Chem B* 121 (2017) 2308-2318.
- [12] N.D. Bernardino, S. Brown-Xu, T.L. Gustafson, D.L.A. de Faria, Time-Resolved Spectroscopy of Indigo and of a Maya Blue Simulant, *J Phys Chem C* 120 (2016) 21905-21914.
- [13] I. Iwakura, A. Yabushita, T. Kobayashi, Why is Indigo Photostable over Extremely Long Periods?, *Chemistry Letters* 38 (2009) 1020-1021.
- [14] I. Iwakura, A. Yabushita, T. Kobayashi, Kinetic isotope effect on the proton-transfer in indigo carmine, *Chem Phys Lett* 484 (2010) 354-357.
- [15] J.M. Seixas de Melo, A. P.; Melo, M. J., Photophysical and Spectroscopic Studies of Indigo Derivatives in Their Keto and Leuco Forms, *J Phys Chem A* 108 (2004) 6975 - 6981.
- [16] R. Rondao, J. Seixas de Melo, M.J. Melo, A.J. Parola, Excited-state isomerization of leuco indigo, *J Phys Chem A* 116 (2012) 2826-2832.
- [17] J.A. Syage, Ultrafast Measurements of Chemistry in Clusters Excited-State Proton Transfer, *J Phys Chem* 99 (1994) 5772 - 5786.
- [18] A.L. Douhal, Françoise; Zewail, Ahmed H., Proton-transfer reaction dynamics, *Chemical Physics* 207 (1996) 477-498.
- [19] G. Meijer, M.S. De Vries, H.E. Hunziker, H.R. Wendt, Laser Desorption Jet-Cooling of Organic Molecules, *Applied Physics B* 51 (1990) 395 - 403.

- [20] F.M. Siouri, S. Boldissar, J.A. Berenbeim, M.S. de Vries, Excited State Dynamics of 6-Thioguanine, *J Phys Chem A* 121 (2017) 5257-5266.
- [21] M.J. Frisch, G.W. Trucks, H.B. Schlegel, G.E. Scuseria, M.A. Robb, J.R. Cheeseman, G. Scalmani, V. Barone, B. Mennucci, G.A. Petersson, H. Nakatsuji, M. Caricato, X. Li, H.P. Hratchian, A.F. Izmaylov, J. Bloino, G. Zheng, J.L. Sonnenberg, M. Hada, M. Ehara, K. Toyota, R. Fukuda, J. Hasegawa, M. Ishida, T. Nakajima, Y. Honda, O. Kitao, H. Nakai, T. Vreven, J.A.M. Jr., J.E. Peralta, F. Ogliaro, M. Bearpark, J.J. Heyd, E. Brothers, K.N. Kudin, V.N. Staroverov, R. Kobayashi, J. Normand, K. Raghavachari, A. Rendell, J.C. Burant, S.S. Iyengar, J. Tomasi, M. Cossi, N. Rega, J.M. Millam, M. Klene, J.E. Knox, J.B. Cross, V. Bakken, C. Adamo, J. Jaramillo, R. Gomperts, R.E. Stratmann, O. Yazyev, A.J. Austin, R. Cammi, C. Pomelli, J.W. Ochterski, R.L. Martin, K. Morokuma, V.G. Zakrzewski, G.A. Voth, P. Salvador, J.J. Dannenberg, S. Dapprich, A.D. Daniels, Ö. Farkas, J.B. Foresman, J.V. Ortiz, J. Cioslowski, D.J. Fox, Gaussian 09, Revision A.2, Gaussian, Inc., Wallingford CT, 2009.
- [22] J. Schirmer, Beyond the Random-Phase Approximation - a New Approximation Scheme for the Polarization Propagator, *Physical Review A* 26 (1982) 2395-2416.
- [23] A.B. Trofimov, J. Schirmer, An Efficient Polarization Propagator Approach to Valence Electron-Excitation Spectra, *Journal of Physics B-Atomic Molecular and Optical Physics* 28 (1995) 2299-2324.
- [24] TURBOMOLE, 2014.
- [25] C. Hättig, F. Weigend, CC2 excitation energy calculations on large molecules using the resolution of the identity approximation, *Journal of Chemical Physics* 113 (2000) 5154-5161.
- [26] A.L. Sobolewski, W. Domcke, C. Hättig, Photophysics of Organic Photostabilizers. Ab Initio Study of the Excited-State Deactivation Mechanisms of 2-(2'-Hydroxyphenyl) benzotriazole, *The Journal of Physical Chemistry A* 110 (2006) 6301-6306.
- [27] W. Siebrand, Radiationless Transitions in Polyatomic Molecules. II. Triplet-Ground-State Transitions in Aromatic Hydrocarbons, *The Journal of Chemical Physics* 47 (1967) 2411-2422.
- [28] A.L. Sobolewski, On the excess-energy dependence of radiationless decay rate constants, *Chemical physics* 115 (1987) 469-479.
- [29] P.M. Felker, A.H. Zewail, Dynamics of intramolecular vibrational-energy redistribution (IVR). II. Excess energy dependence, *The Journal of chemical physics* 82 (1985) 2975-2993.
- [30] P.M. Felker, A.H. Zewail, Observation of restricted IVR in large molecules: Quasi-periodic behavior, phase-shifted and non-phase-shifted quantum beats, *Chem Phys Lett* 102 (1983) 113-119.

Supplemental information

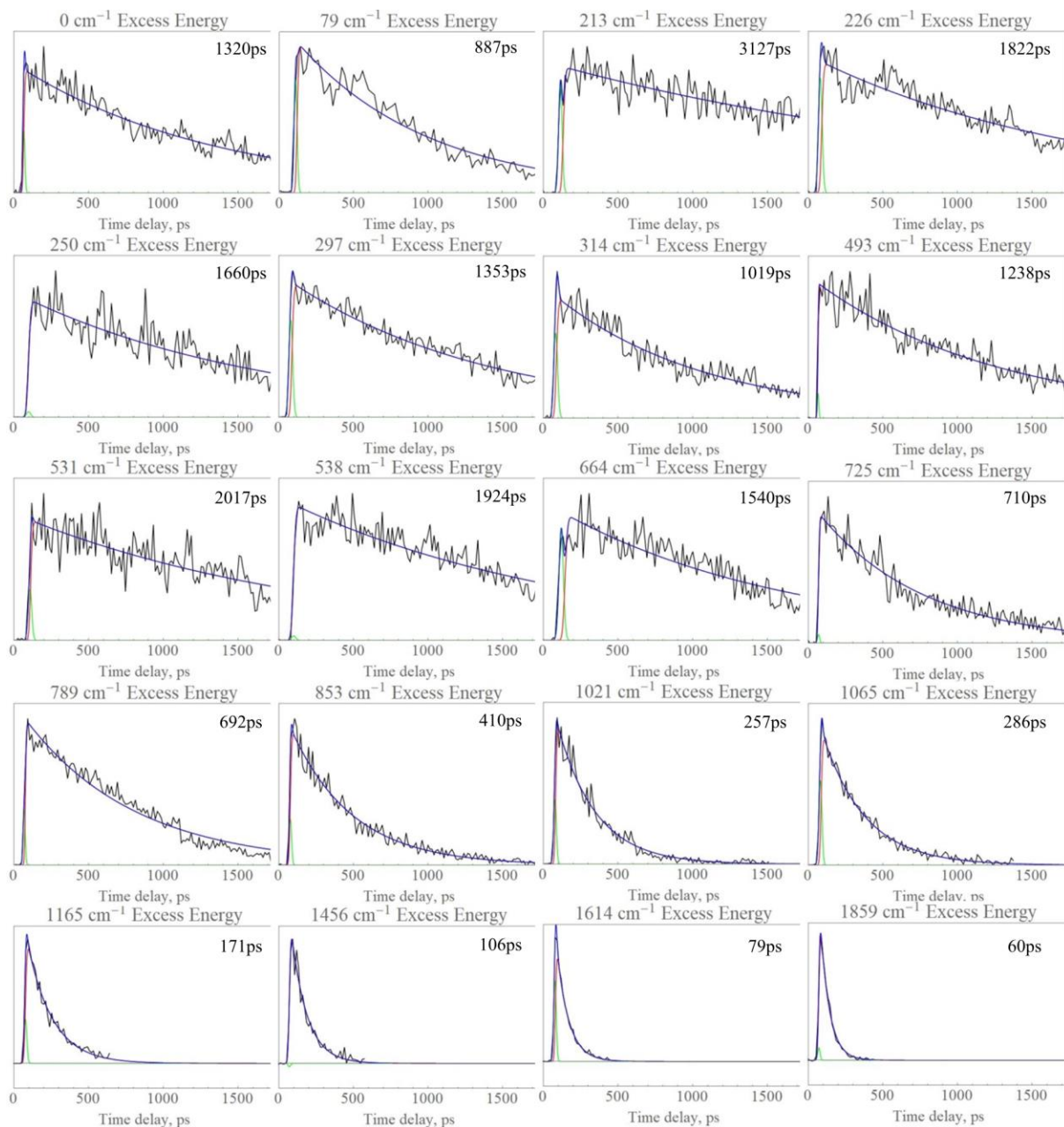


Figure S1. The pump probe transients from the ps pump probe experiments (OPG + 213) with the derived lifetime values. Data is in black, IRF in green, the decaying component in red, and the total fit in blue.

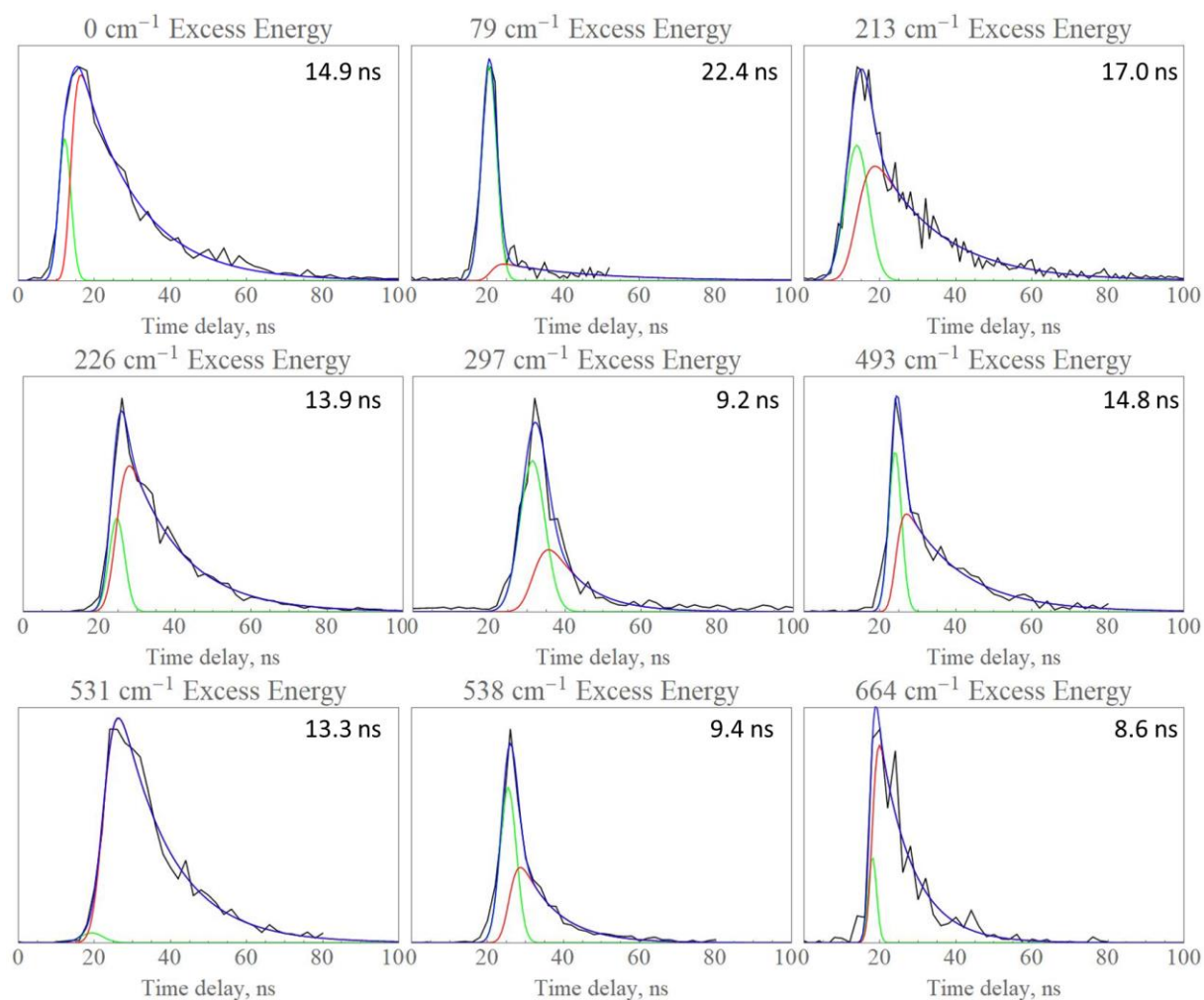


Figure S2. The pump probe transients from the ns pump probe experiments (OPG + 193nm) with the derived lifetime values. Data is in black, IRF in green, the decaying component in red, and the total fit in blue.

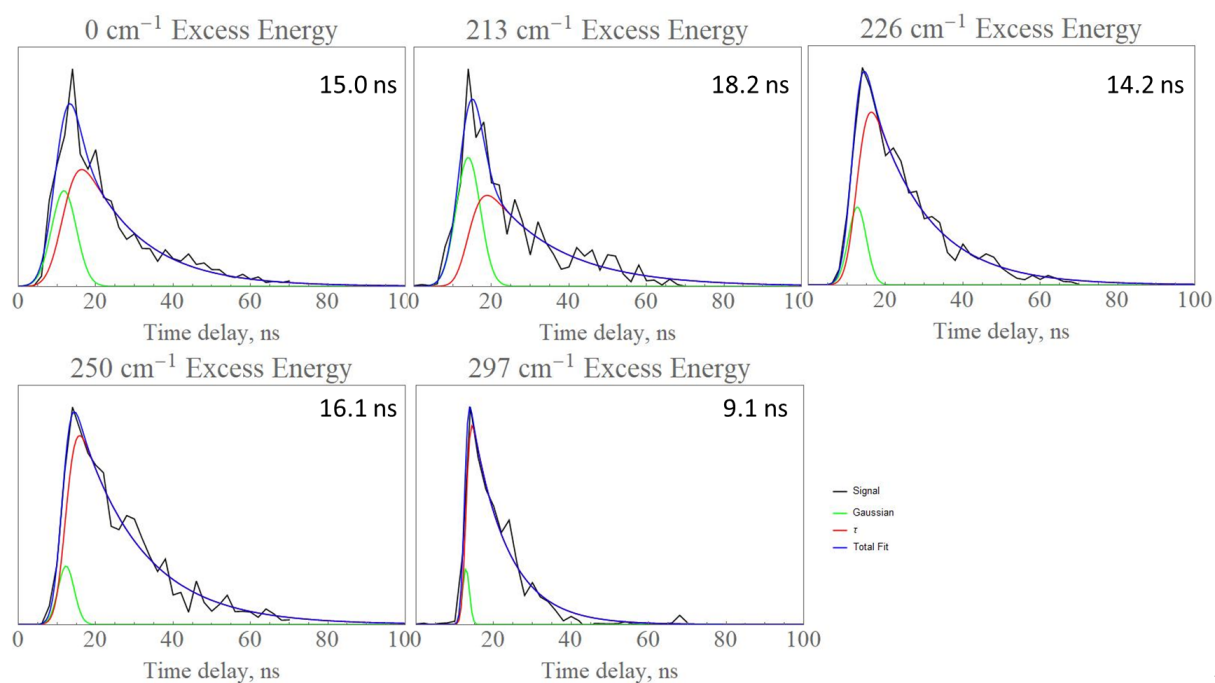


Figure S3. The pump probe transients from the ns pump probe experiments (dye + 213 nm) with the derived lifetime values. Data is in black, IRF in green, the decaying component in red, and the total fit in blue.

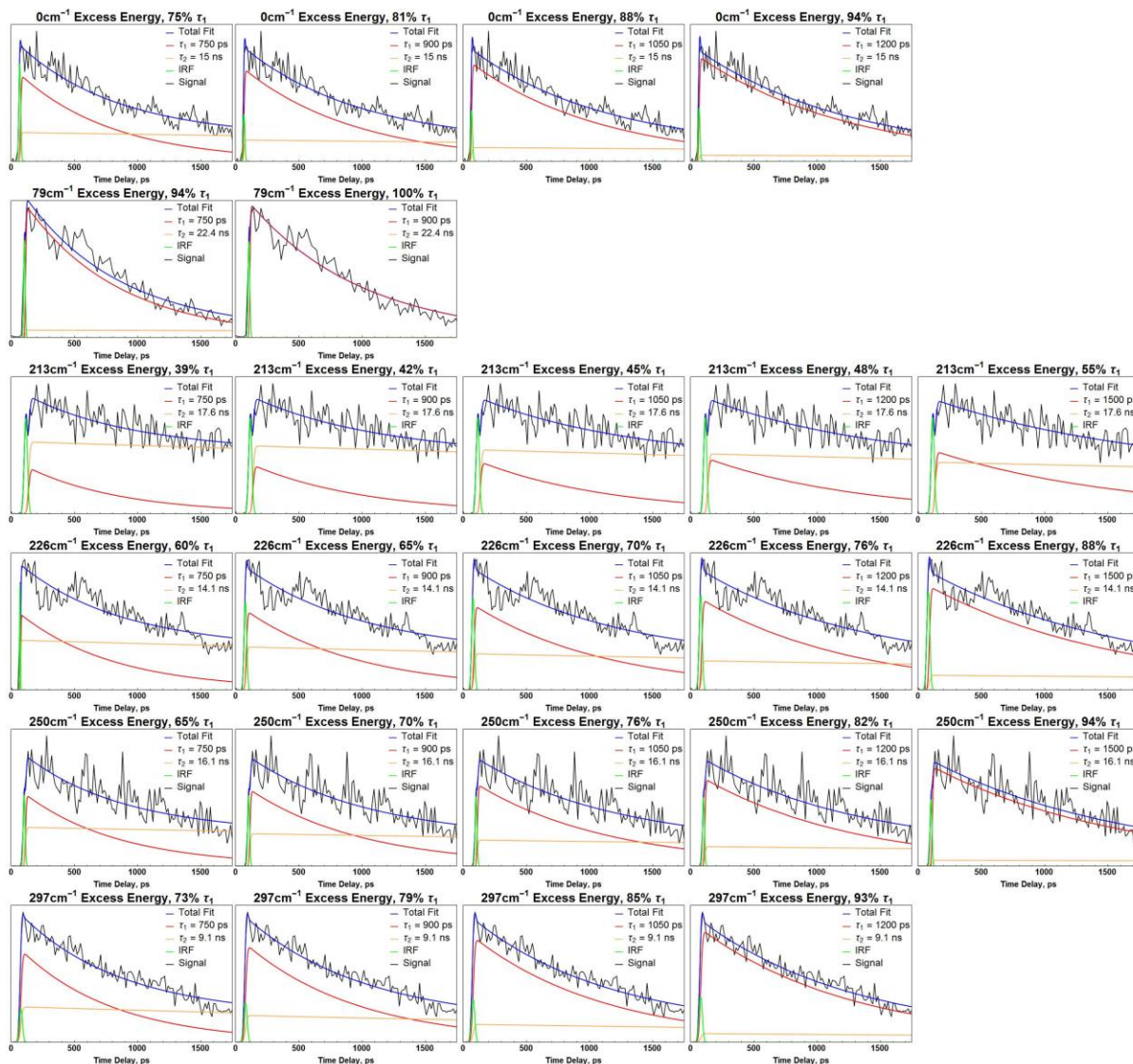


Figure S4a. The first 6 peaks of spectral range A with the different permutations of lifetime values fit in order to derive the range of possible relative quantum yields.

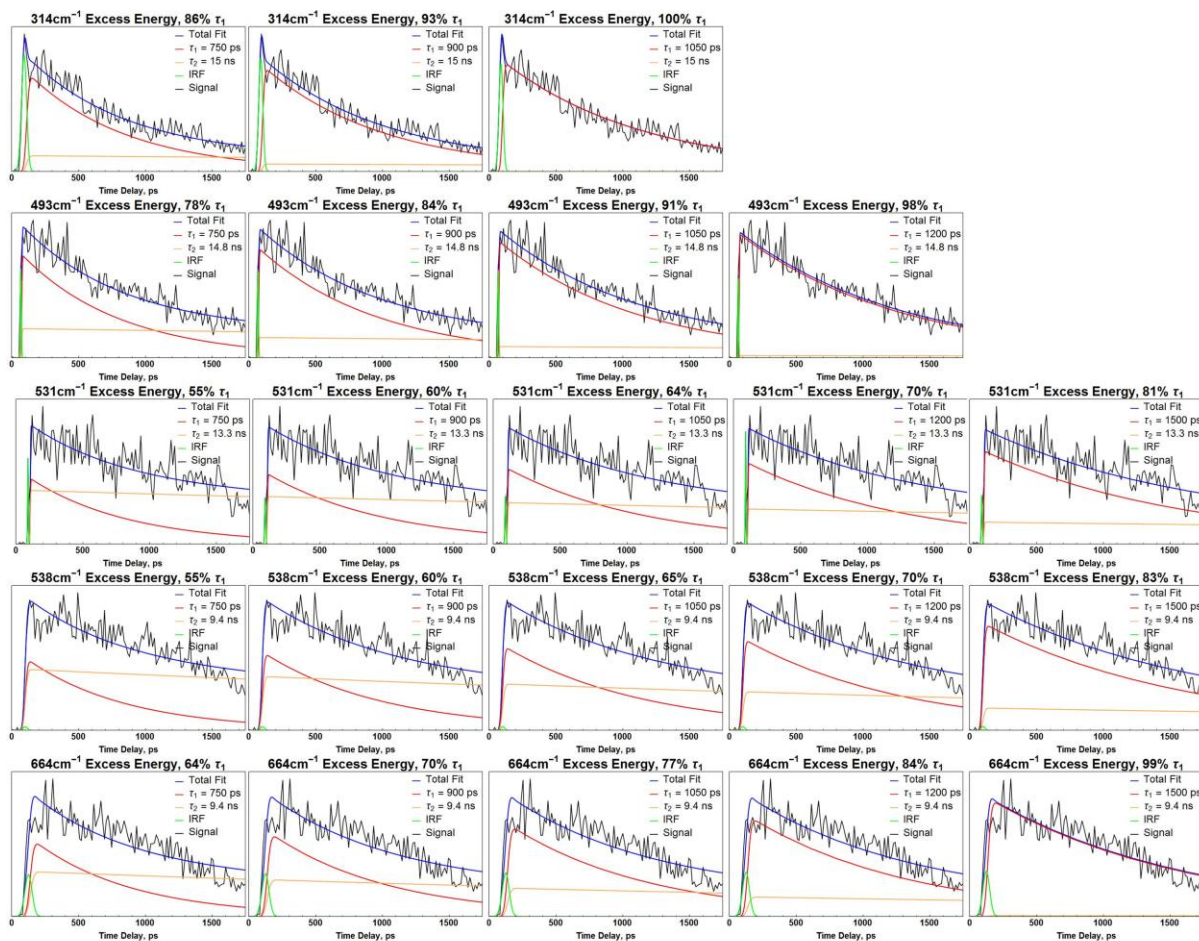


Figure S4b. The latter 5 peaks of spectral range A with the different permutations of lifetime values fit in order to derive the range of possible relative quantum yields.

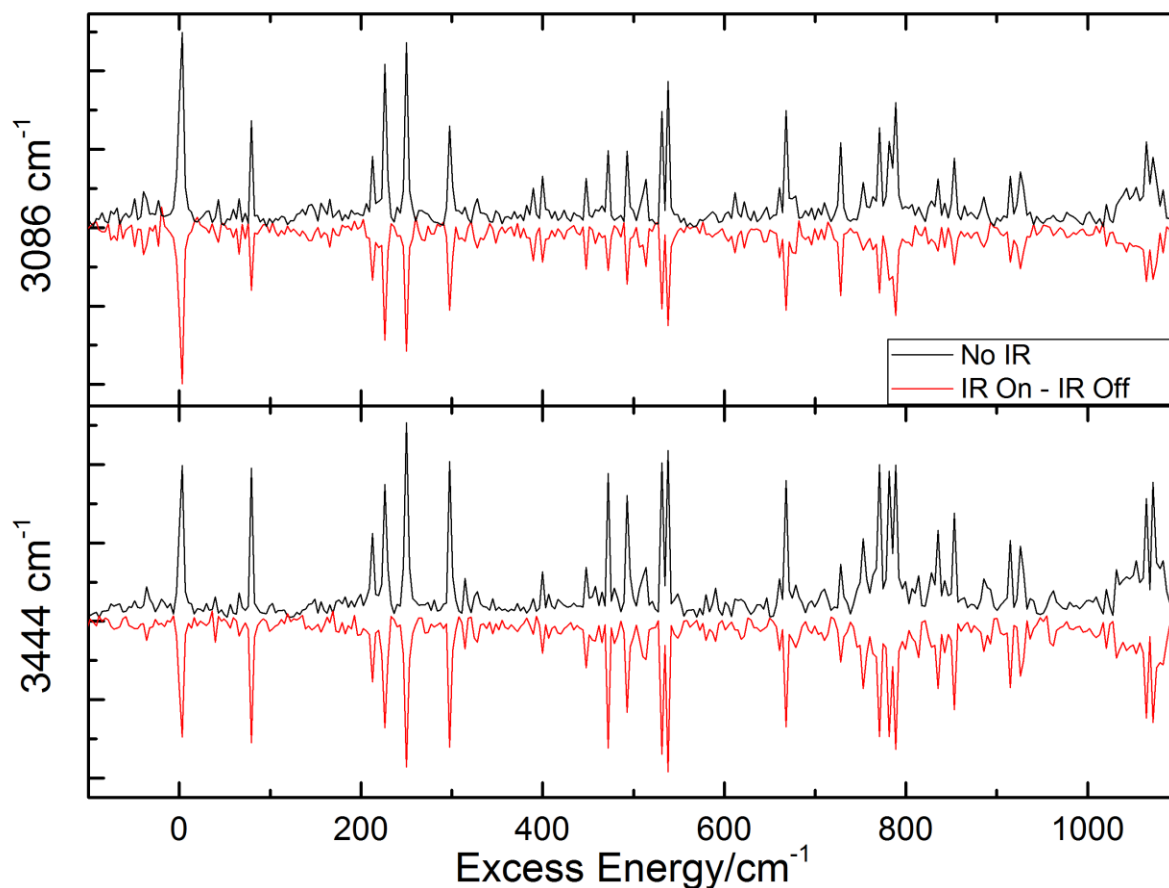


Figure S5. IR-Vis double resonance spectroscopy mode II of indigo with burn pulses set at a) 3084 and b) 3444 cm^{-1} , while probing with 2C from 18018 – 19230 cm^{-1} (555 – 520 nm, ps opg + 213). Burn on and burn off spectra were generated again using a digital chopper

Table S1a. Vertical transition energy (ΔE), oscillator strength (f), dipole moment (μ), and leading electronic configurations of indigo computed with ADC(2)/cc-pVDZ method at the MP2/cc-pVDZ equilibrium geometry of the $S_0(\text{KK})$ state. Numbers in the figure denote bondlengths in Angstrom.

State	ΔE /eV	f	μ /Debye	el. config.
S_0	0.0	-	0.0	$(29ag)^2(5bg)^2(6au)^2(28bu)^2$
$S_1(\pi\pi^*)$	2.203	0.351	0.0	$0.97(6au-6bg)$
$S_2(n\pi^*)$	2.901	0.0	0.0	$0.94(29ag-6bg)$
$S_3(\pi\pi^*)$	3.185	0.0	0.0	$0.90(5bg-6bg)$

Table S1b. Relevant molecular orbitals involved into the lowest electronic excitations of the $S_0(KK)$ state of indigo.

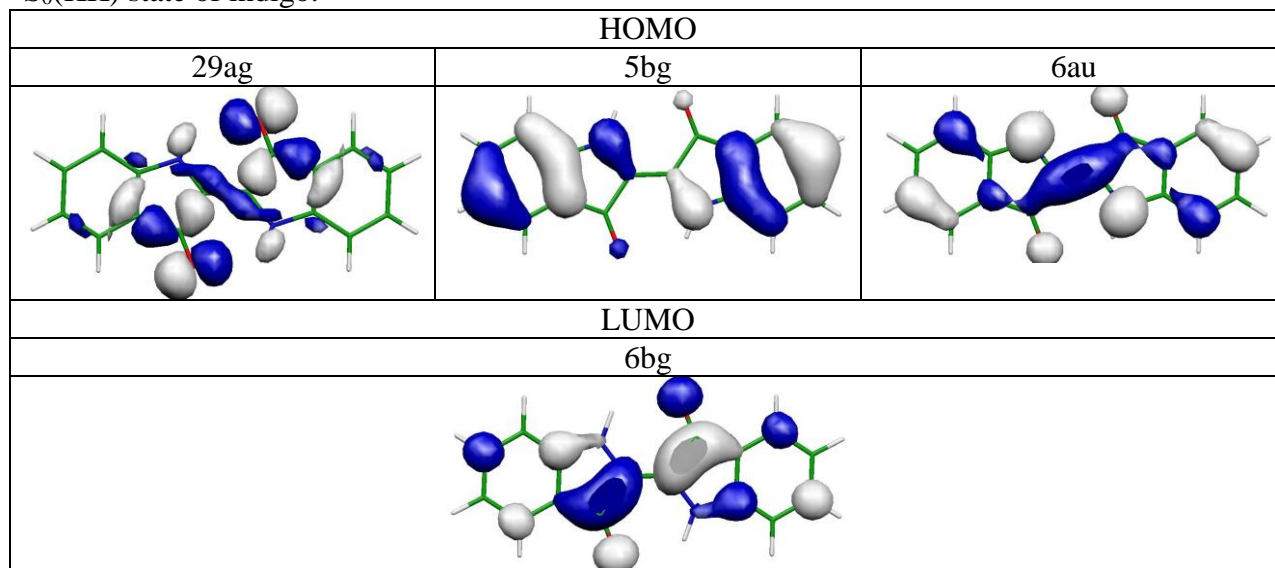
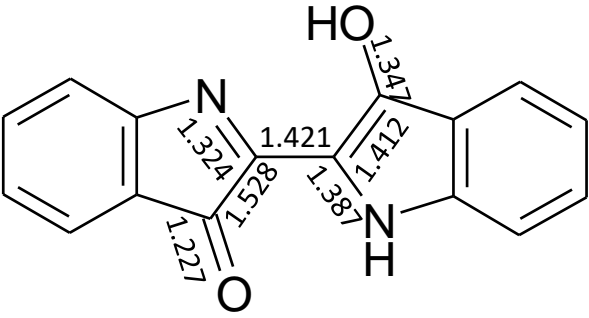


Table S2a. Vertical transition energy (ΔE), oscillator strength (f), dipole moment (μ), and leading electronic configurations of indigo computed with ADC(2)/cc-pVDZ method at the MP2/cc-pVDZ equilibrium geometry of the S_0 (EK) state. Numbers in the figure denote bondlengths in Angstrom.



State	ΔE /eV	f	μ /Debye	μ_x /Debye	μ_y /Debye	el. config.
S_0	(0.126) ^a	-	1.40	-1.11	-0.86	$(57a')^2(11a'')^2$
$S_1(\pi\pi^*)$	2.101	0.290	6.45	6.09	2.12	$0.95(11a''-12a'')$
$S_2(n\pi^*)$	2.681	0.0	3.03	-0.89	2.89	$0.92(57a'-12a'')$
$S_3(\pi\pi^*)$	3.000	0.046	7.73	7.73	0.13	$0.91(10a''-12a'')$

a) Relative to energy of the KK tautomer.

Table S2b. Relevant molecular orbitals involved into the lowest electronic excitations of the S_0 (EK) state of indigo.

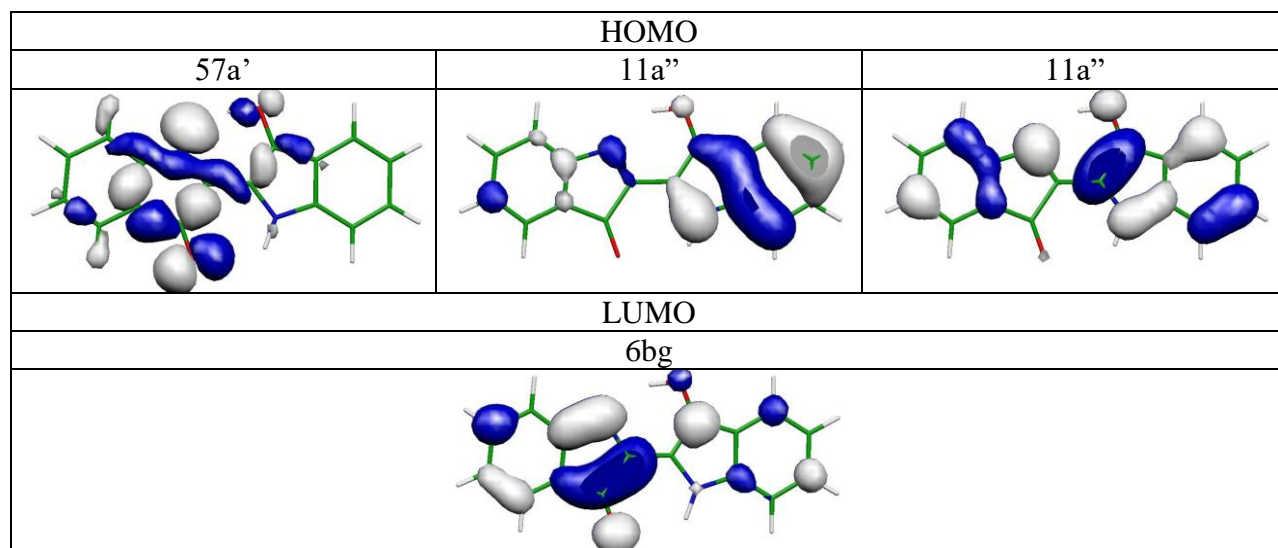
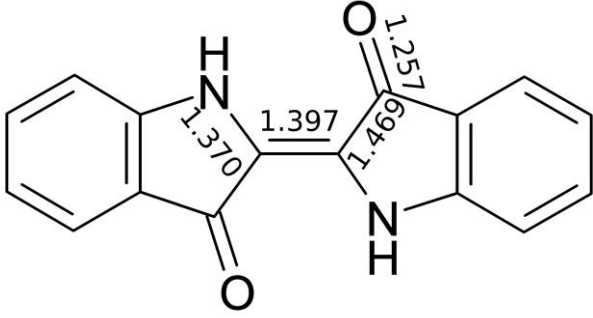


Table S3a. Transition energy (ΔE), oscillator strength (f), dipole moment (μ), and leading electronic configurations of indigo computed with ADC(2)/cc-pVDZ method at the S_1 (KK)-state equilibrium geometry. Numbers in the figure denote bondlengths in Angstrom.

				
State	ΔE \eV	f	μ /Debye	el. config.
S_0	0.111 ^a	-	0.0	$(35a)^2(33b)^2$
$S_1(\pi\pi^*)$	2.087 ^b	0.289	0.0	$0.97(35a-34b)$

a) Vertical energy computed at the equilibrium geometry of the S_1 state.

b) Adiabatic energy relative to the energy of the KK tautomer.

Table S3b. Relevant molecular orbitals involved into the lowest electronic excitation of the S_1 (KK) state of indigo.

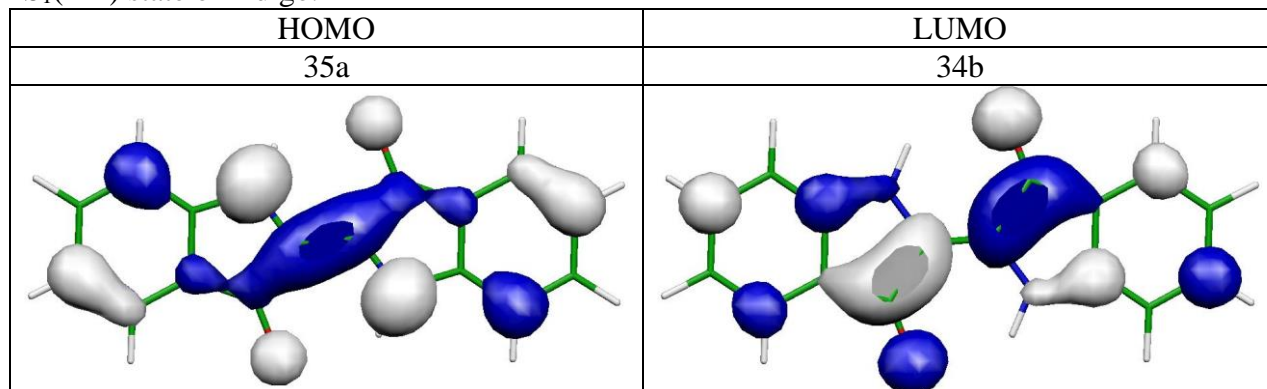
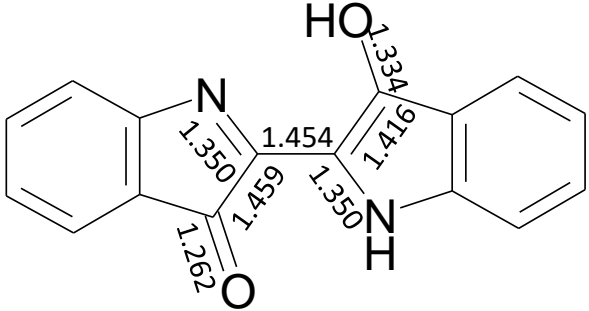


Table S4a. Transition energy (ΔE), oscillator strength (f), dipole moment (μ), and leading electronic configurations of indigo computed with ADC(2)/cc-pVDZ method at the $S_1(\text{EK})$ -state equilibrium geometry of the X conformer. Numbers in the figure denote bondlengths in Angstrom.

						
State	$\Delta E/\text{eV}$	f	μ/Debye	μ_x/Debye	M_y/Debye	el. config.
S_0	0.436 ^a	-	1.27	-1.14	-0.55	$(57a')^2(11a'')^2$
$S_1(\pi\pi^*)$	1.901 ^b	0.198	6.77	6.39	2.22	$0.96(11a''-12a'')$

a) Vertical energy computed at the equilibrium geometry of the S_1 state.

b) Adiabatic energy relative to the energy of the KK tautomer.

Table S4b. Relevant molecular orbitals involved into the lowest electronic excitation of X conformer.

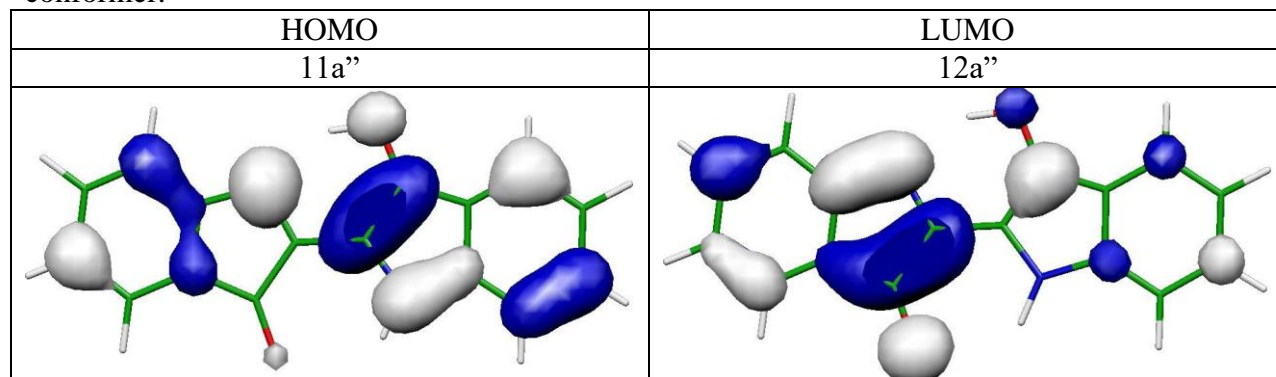
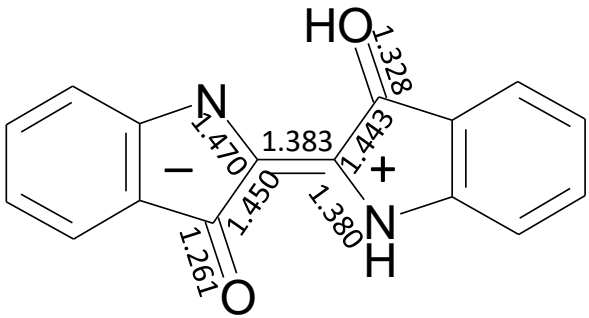


Table S5c. Cartesian coordinates of the X conformer optimized in the S1 state with ADC(2)/cc-pVDZ method.

FINAL HEAT OF FORMATION = -873.0870932672

C	0.6619206	-0.1065775	0.0000000
C	-0.7917185	-0.1084148	0.0000000
N	-1.3985199	1.0978465	0.0000000
C	-2.7676758	0.7926254	0.0000000
C	-3.0043410	-0.6229450	0.0000000
C	-1.6739363	-1.2707338	0.0000000
C	-4.3142052	-1.1177566	0.0000000
C	-5.3770140	-0.1899119	0.0000000
C	-5.1448470	1.2060598	0.0000000
C	-3.8331444	1.7110423	0.0000000
O	-1.3062324	-2.4778345	0.0000000
N	1.4125181	-1.2288768	0.0000000
C	2.7734972	-0.8846437	0.0000000
C	2.8619550	0.5460147	0.0000000
C	1.5072170	1.0297627	0.0000000
C	4.1264700	1.1661229	0.0000000
C	5.2664726	0.3450092	0.0000000
C	5.1626702	-1.0629600	0.0000000
C	3.9040704	-1.7000052	0.0000000
O	1.0762926	2.2921322	0.0000000
H	-3.6331386	2.7883907	0.0000000
H	-5.9945195	1.8969170	0.0000000
H	-6.4098504	-0.5563297	0.0000000
H	-4.5014013	-2.1971141	0.0000000
H	0.0717783	2.2060724	0.0000000
H	0.9634197	-2.1519527	0.0000000
H	3.8209729	-2.7918052	0.0000000
H	6.0707347	-1.6740663	0.0000000
H	6.2591344	0.8066818	0.0000000
H	4.2114206	2.2572504	0.0000000

Table S5a. Transition energy (ΔE), oscillator strength (f), dipole moment (μ), and leading electronic configurations of indigo computed with ADC(2)/cc-pVDZ method at the S_1 (EK)-state equilibrium geometry of the Y conformer. Numbers in the figure denote bondlengths in Angstrom.



State	ΔE /eV	f	μ /Debye	μ_x /Debye	μ_y /Debye	el. config.
S_0	1.035 ^a	-	4.14	4.13	-0.31	$(57a')^2(11a'')^2$
$S_1(\pi\pi^*)$	1.875 ^b	0.097	3.39	-2.71	2.04	$0.96(11a''-12a'')$

a) Vertical energy computed at the equilibrium geometry of the S_1 state.

b) Adiabatic energy relative to the energy of the KK tautomer.

Table S5b. Relevant molecular orbitals involved into the lowest electronic excitations of Y conformer.

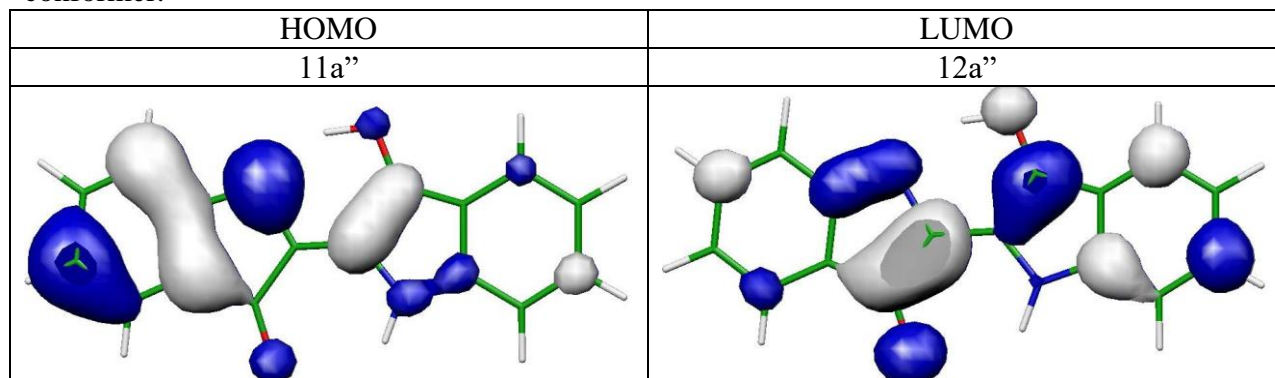


Table S6c. Cartesian coordinates of the Y conformer optimized in the S1 state with ADC(2)/cc-pVDZ method.

FINAL HEAT OF FORMATION = -873.0879616948

```

C  0.6302364 -0.1642869  0.0000000
C -0.7531914 -0.1667760  0.0000000
N -1.4278622  1.1395201  0.0000000
C -2.7255052  0.8057657  0.0000000
C -2.9679095 -0.6339839  0.0000000
C -1.6575612 -1.3006363  0.0000000
C -4.2757554 -1.1395843  0.0000000
C -5.3411587 -0.2273084  0.0000000
C -5.1204606  1.1893114  0.0000000
C -3.8366860  1.7139106  0.0000000
O -1.3439359 -2.5217731  0.0000000
N  1.4343001 -1.2862716  0.0000000
C  2.7560221 -0.8932104  0.0000000
C  2.8189884  0.5455082  0.0000000
C  1.4724280  1.0078886  0.0000000
C  4.0708499  1.2087497  0.0000000
C  5.2288439  0.4311086  0.0000000
C  5.1562485 -0.9887962  0.0000000
C  3.9300460 -1.6663927  0.0000000
O  1.0400652  2.2639112  0.0000000
H -4.4463235 -2.2216296  0.0000000
H -6.3718698 -0.5984008  0.0000000
H -5.9849861  1.8617724  0.0000000
H -3.6511799  2.7931817  0.0000000
H  0.0376944  2.1858199  0.0000000
H  1.0332802 -2.2236377  0.0000000
H  3.8876461 -2.7604011  0.0000000
H  6.0836323 -1.5718356  0.0000000
H  6.2101154  0.9159788  0.0000000
H  4.1139886  2.3024977  0.0000000

```

X form	Y form
--------	--------

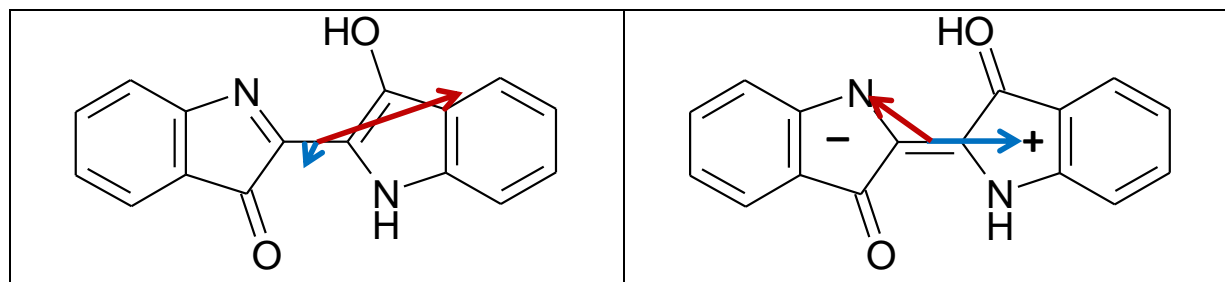


Fig. S6. Geometric structures of the X and Y enol-keto forms of indigo with the electronic structures indicated. Arrows illustrate direction and value of dipole moments computed for the S_0 state (blue) and for the S_1 state (red) at the S_1 -optimized geometry.